ACS APPLIED MATERIALS & INTERFACES

Research Article

www.acsami.org

Electrochemical Codeposition of Vanadium Oxide and Polypyrrole for High-Performance Supercapacitor with High Working Voltage

Ming-Hua Bai, Li-Jun Bian, Yu Song, and Xiao-Xia Liu*

Department of Chemistry, Northeastern University, Shenyang, 110819, China

ABSTRACT: Electrochemical codeposition of vanadium oxide (V_2O_5) and polypyrrole (PPy) is conducted from vanadyl sulfate ($VOSO_4$) and pyrrole in their aqueous solution to get V_2O_5−PPy composite, during which one-dimensional growth of polypyrrole (PPy) is directed. X-ray diffraction (XRD) and Fourier transform infrared spectroscopy (FT-IR) are used to characterize the composite, while scanning electron microscopy (SEM) is used to investigate their morphologies. Cyclic voltammetry (CV), chronopotentiometry (CP) for galvanostatic charge−discharge and electrochemical impedance spectroscopy (EIS) are used to study electrochemical activities and pseudocapacitive properties of the composite. The influences of $VOSO_4$ to pyrrole ratio in the electrocodeposition solution on morphologies and pseudocapacitive properties of the composite are discussed. Due to the organic−inorganic synergistic effect, V_2O_5−PPy composite exhibits good charge-storage properties in a large potential window from −1.4 to 0.6 V vs SCE, with a specific capacitance of 412 F/g at 4.5 mA/cm^2. A model supercapacitor assembled by using the V_2O_5−PPy composite as the electrode materials displays a high operating voltage of 2 V and so a high energy density of 82 Wh/kg (at the power density of 800 W/kg).

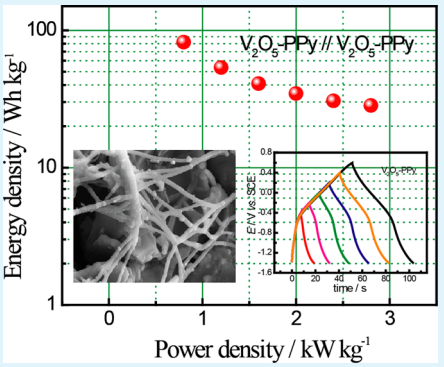

KEYWORDS: *vanadium oxide, polypyrrole, electro-codeposition, supercapacitor*

INTRODUCTION

Electrochemical capacitor (supercapacitor) is a very potential energy storage device with the advantage of high power density, long cycle life and comparable energy density. However, to meet the increasing demand for energy storage, significant increase of energy density for supercapacitor is still a great challenge.[1−3] Specific capacitance (C_m) and operating voltage (U) of capacitor are two key parameters for its energy density (E) according to $E = 1/2C_mU^2$. Transition metal oxides and conducting polymers display higher capacitance than carbon based materials as they can store charge through highly reversible redox reactions.[4] However, most of these pseudocapacitive materials usually can only store charge in narrow positive potential range. So the operating voltage of capacitors assembled by these electrode materials is very limited, directing to low energy density. Carbon materials can store charge in both positive and negative potential range, resulting in high working voltage for the assembled supercapacitors. However, they usually display relatively low specific capacitance as charges are mainly accumulated through electrical double-layer, which restricts the energy density of the assembled supercapacitor.[5−8] Although asymmertric supercapacitors can be assembled by using carbon and pseudocapacitive materials as negative and positive electrodes, respectively to increase the opterating voltage, the specific capacitance of the capacitor is limited by the carbon material which has small capacitance ($1/C = 1/C_{an} + 1/C_{cat}$; C_{an}: capacitance of anode; C_{cat}: capacitance of cathode). An anode with comparable energy density to cathode is essential for high energy density supercapacitors. However, pseudocapacitive anode is less developed.

Some of the transitional metal oxides like vanadium oxide and indium oxide display electroactivities in negative potentials and so can be used as anodes for high operating voltage supercapacitors.[9−11] Multiple stable oxidation states are accessible for vanadium in its oxide which has layered structure and so allows efficient ion diffusion.[12,13] So vanadium oxide has attracted much attention for charge storage. The electro-spun V_2O_5 nanofibers was reported to exhibit good charge storage behaviors from −1 to 0 V vs SCE.[10] A core−shell nanocomposite of V_2O_5 and polypyrrole displayed a high specific capacitance of 308 F/g (at a current density of 0.1 A/g) from −0.9 to 0.1 V vs SCE.[14] It is anticipated that V_2O_5 can be a good candidate for supercapacitor anode. However, similar to other inorganic oxides, low electrical conductivity and less efficient pseudocapacitive contribution restrict its application in high performance supercapacitors.

Composite nanowires of V_2O_5-polyaniline (PANI) were synthesized in our previous work.[15] In the supercapacitor assembled by using the composite as both of the electrode materials, the oxide mainly contributed to charge storage in negative potentials while the charge storage in positive potentials was mainly devoted by the polymer. This is very like the type III polymer supercapacitor,[16] in which both of the

Received: April 30, 2014
Accepted: July 10, 2014
Published: July 10, 2014

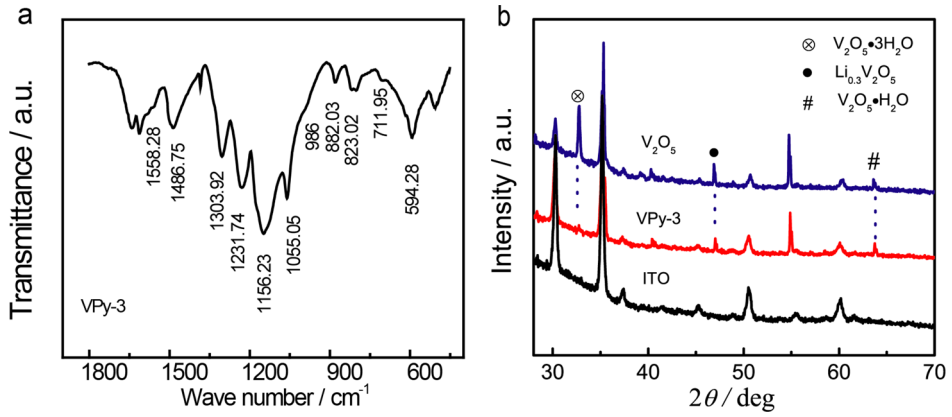

Figure 1. (a) FT-IR spectrum of VPy-3. (b) XRD spectra collected for V_2O_5 and VPy-3 deposited on ITO together with that of ITO; characteristic diffraction peaks of $V_2O_5{\cdot}3H_2O$, $Li_{0.3}V_2O_5$, and $V_2O_5{\cdot}H_2O$ are highlighted by dashed lines.

electrode materials are the same polymer which can be *p*-doped as well as *n*-doped. When charged, one polymer electrode is fully *n*-doped and the other polymer electrode is fully *p*-doped, so in fact this is an asymmetric supercapaciotor as charges are stored through different electrochemistry processes. This kind of supercapacitor can operate with a high working voltage as the *p*-doping and *n*-doping occurs in quite different potentials. Due to the combined electroactivities of the oxide in negative potentials and the polymer in the positive potentials, our type III composite supercapacitor V_2O_5–PANI//V_2O_5–PANI displayed a high operating voltage of 1.6 V and so an excellent energy density of 69.2 Wh/kg.

Polypyrrole (PPy) is an important conducting polymer which displays good pseudocapacitive behaviors in neutral aqueous solutions.[17,18] Moreover, PPy displayed both anion-involved and cation-involved electrochemistry processes (dual mode) which occur in quite different potential range (−0.8 to 0.5 V vs SCE), leading to wide potential window for charge storage.[19] To get new electrode materials for type III composite supercapacitors with high working voltage and enhanced charge storage properties, electrochemical codeposition of vanadium oxide and PPy was conducted in this work to afford V_2O_5–PPy composites. One-dimensional growth of PPy was directed through this electro-codeposition with V_2O_5 to endue the obtained composite large contacted surface area with the electrolyte for high charge storage performance. There is no other report about PPy one-dimensional growth directed by electro-codeposition with inorganic oxides, to the best of the authors' knowledge, as fibrillar structure is not intrinsic for PPy and so it is very hard for this polymer to grow one-dimensionally.[20] The composite displayed a large charge storage potential window of 2.0 V from −1.4 to 0.6 V vs SCE with a high specific capacitance of 412 F/g at 4.5 mA/cm^2. A type III supercapacitor was assembled by using the composite as both of the anode and cathode, which achieved an energy density of 82 Wh/kg at the power density of 800 W/kg.

EXPERIMENTAL SECTION

Materials. Pyrrole (Py) was distilled prior to use. All other chemicals were of analytical grade and used as received. Carbon cloth (SGL group, German) and a saturated calomel electrode (SCE) were used as counter electrode and reference electrodes, respectively in three-electrode electrolytic cell for electrodeposition and electrochemical property studies of V_2O_5–PPy composites.

Electrodeposition of V_2O_5–PPy Composite, V_2O_5, and PPy Films on Carbon Cloth. Electrodeposition was conducted on a piece of carbon cloth with a geometric area of 1.5*1.5 cm^2 which was primarily cyclic voltammetric scanned from −1.2 to 2.0 V vs SCE at 100 mV s^{-1} in 2.0 M H_2SO_4 to remove surface contamination. Electrocodeposition of V_2O_5–PPy composite was conducted by potentiosatic method at 0.7 V vs SCE from a 0.1 mol L^{-1} phosphate buffer solution (pH 6.864) containing 0.1 mol L^{-1} $LiClO_4$, 0.1 M vanadyl sulfate ($VOSO_4$) and 0.03 M pyrrole, in which the mole ratio of $VOSO_4$ to pyrrole is 3:1 and so the obtained film was denoted as VPy-3. The deposition was kept until 1.5 mAh charges passed the working electrode to control the loading of the composite to be 1.20 mg. For comparison, V_2O_5 and PPy were prepared in solutions containing 0.1 M $VOSO_4$ and 0.03 M pyrrole, respectively under the same conditions.

To investigate the influence of $VOSO_4$ to pyrrole ratio on the electrochemical codeposition of V_2O_5 and PPy, composite films of VPy-1, VPy-2, VPy-4 and VPy-5 were similarly prepared from solutions containing 0.1 M $VOSO_4$ and 0.1, 0.05, 0.025, 0.02 M pyrrole, in which the mole ratio of $VOSO_4$ to pyrrole is 1:1, 2:1, 4:1, 5:1, respectively.

Fabrication of Type III Composite Supercapacitor of VPy-3// VPy-3. The type III composite supercapacitor was assembled by using two pieces of VPy-3 composite electrodes as anode and cathode, respectively and LiCl/PVA gel as the electrolyte, similar to our previously reported supercapacitor assembly by using gel electrolyte.[15] The working area of the type III composite supercapacitor was 1.5*1.5 cm^2 and the total mass loading of the two electrodes was 2.40 mg.

Material Characterization. Fourier transform infrared spectroscopy (FT-IR, A Spectrum One, PerkinElmer, USA), X-ray diffraction (XRD, PW3040/60, PANalytical B.V., Netherlands) and energy-dispersive X-ray spectroscopy (EDX, EVO18, Carl Zeiss, Germany) were used to determine the sample content of the composite. Morphologies were investigated by scanning electron microscope (SEM, EVO18, Carl Zeiss, Germany). Electrochemical property study was conducted in 5 M LiCl by cyclic voltammetry (CV), galvanostatic charge–discharge from −1.4 to 0.6 V vs SCE. Electrochemical impedance measurements were carried out at open circuit potential in a frequency range of 100 mHz to 40 kHz with a perturbation of 10 mV, using VMP3 multichannel electrochemical analyzer system (Bio-Logic-Science Instruments, France). Mass loading was measured by Sartorius BT25s semimicro balance (d = 0.01 mg).

RESULTS AND DISCUSSION

The chemical component of the as-synthesized V_2O_5–PPy composite VPy-3 was first analyzed by FT-IR (Figure 1a). Typical vibrations of PPy and V_2O_5 can be seen in the spectrum, for example those at 1558.28 and 1486.75 cm^{-1} for typical absorption peaks of pyrrole ring.[21−23] The C–N vibration appears at 1303.92 and 1231.74 cm^{-1}.[22,23] The bands at 1156.23 and 882.03 cm^{-1} can be assigned to the in-plane and out-of-plane deformations of $(C–H)_{ar}$.[21,22] While the

dx.doi.org/10.1021/am502630g | ACS Appl. Mater. Interfaces 2014, 6, 12656−12664

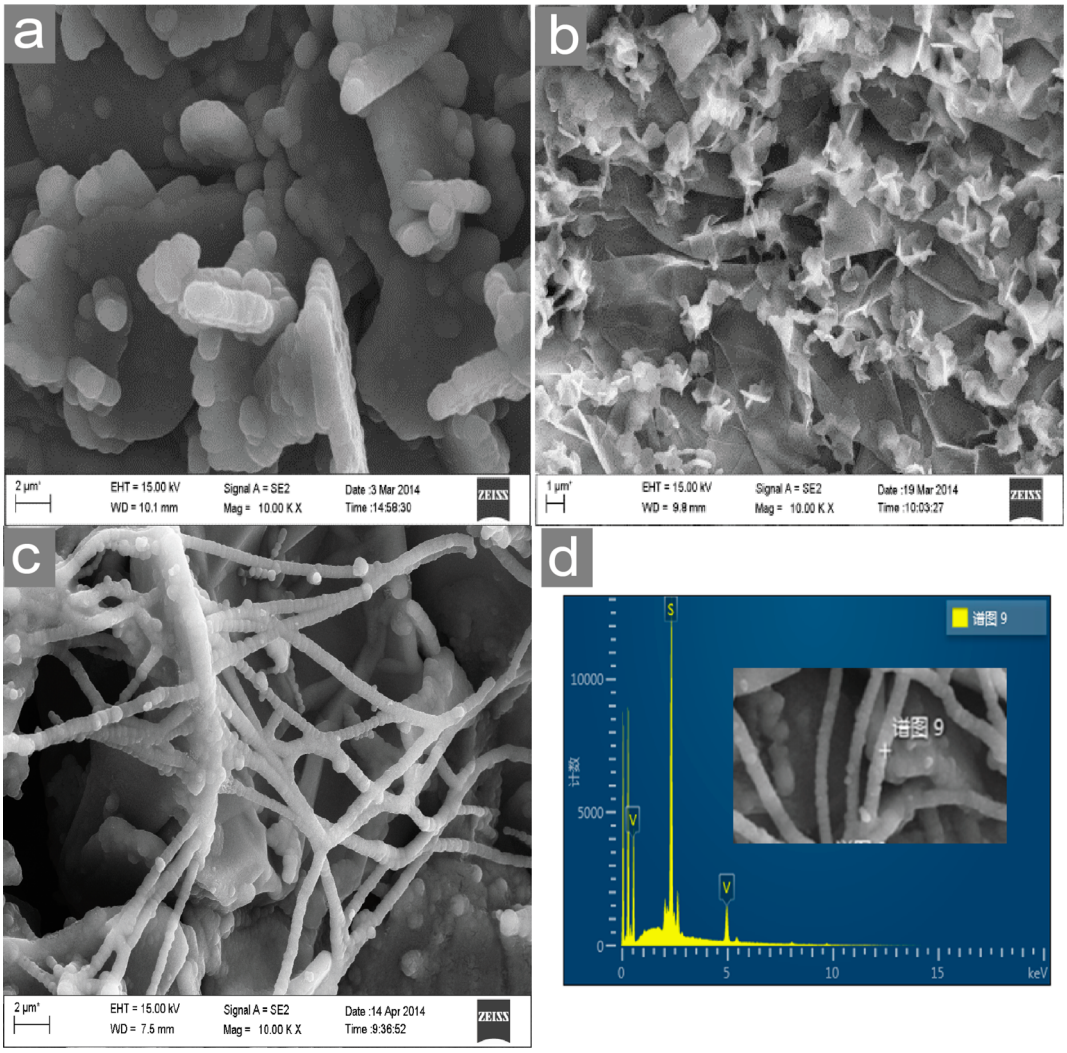

Figure 2. SEM images of (a) PPy, (b) V_2O_5, and (c) VPy-3 deposited on carbon cloth substrate. (d) EDX spectrum of VPy-3 spot analyzed on a nanofiber; (inset) SEM image with the analysis spot marked.

vibration at 1055.05 cm^{-1} is characteristic of in-plane deformation of (N−H) in the pyrrolic nucleus.[21] The V═O stretching is overlapped with this (N−H) in-plane deformation and displays as a shoulder peak at 986 cm^{-1}. The bands at 823.02 and 594.28 cm^{-1} correspond to the V−O−V bending vibration and edge-sharing vibration, respectively. The V−OH_2 stretching mode appears at 711.95 cm^{-1}, indicating that there is coordinated H_2O in the structure.[24]

XRD measurement is conducted on VPy-3 which was similarly electrodeposited on ITO glass. The XRD patterns of VPy-3 and similarly prepared V_2O_5 are in Figure 1b, together with those of ITO. On both of the XRD patterns of VPy-3 and V_2O_5, except signals of ITO, diffractions can be seen at 32.58°, 46.89° and 63.69° which corresponding to crystalline structures of $V_2O_5{\cdot}3H_2O$, $Li_{0.3}V_2O_5$ and $V_2O_5{\cdot}H_2O$, respectively (JSPDS card No. 07−0332, 18−0755 and 41−1426).[10,15] This indicates that some water molecules coordinated in the oxide and also there are some Li^+ ions inserted in the oxide through electrodeposition from solutions containing $LiClO_4$.

Morphologies of PPy, V_2O_5 and VPy-3 samples are investigated by SEM (Figure 2). Pure PPy forms irregular-shaped particles on carbon cloth (Figure 2a). Similar to the one-dimensional directing of PANI by electro-codeposition with V_2O_5 to form V_2O_5−PANI composite nanowires,[15] one-dimensional growth of PPy emerged to form nanofibrous composite in VPy-3 (Figure 2c), supported by signals of element V from V_2O_5 and element S from doping anion in PPy on EDX spectrum spot-analyzed on a nanofiber of VPy-3 (Figure 2d). Unlike PANI to which the fibrillar polymer is intrinsic, it is very hard for PPy to grow one dimensionally.[20] Although nanofibrous PANI can be successfully synthesized by aqueous/organic interfacial polymerization,[25] rapidly mixed reaction,[26] ultrasonic irradiation,[27] dilute polymerization,[28] etc., only nonfibrous, granular powders of PPy can be obtained by these approaches.[20] While there are several reports describing the one-dimensional growth of PPy through hard and soft templates[29,30] as well as reactive seed templates,[20] there is no report about PPy one-dimensional growth directed by electro-codeposition with inorganic oxides, to the best of the authors' knowledge. When electro-codeposited with V_2O_5, the freshly formed oxide may act as reactive seed to direct one-dimensional grow for PPy.[20] The incorporation of V_2O_5 will also be helpful to avoid the PPy chain entanglement and the irregular particle formation. This one-dimensional grown composite with large surface area may facilitate the effect contact of their reactive centers with electrolyte and the charge transfer as well.

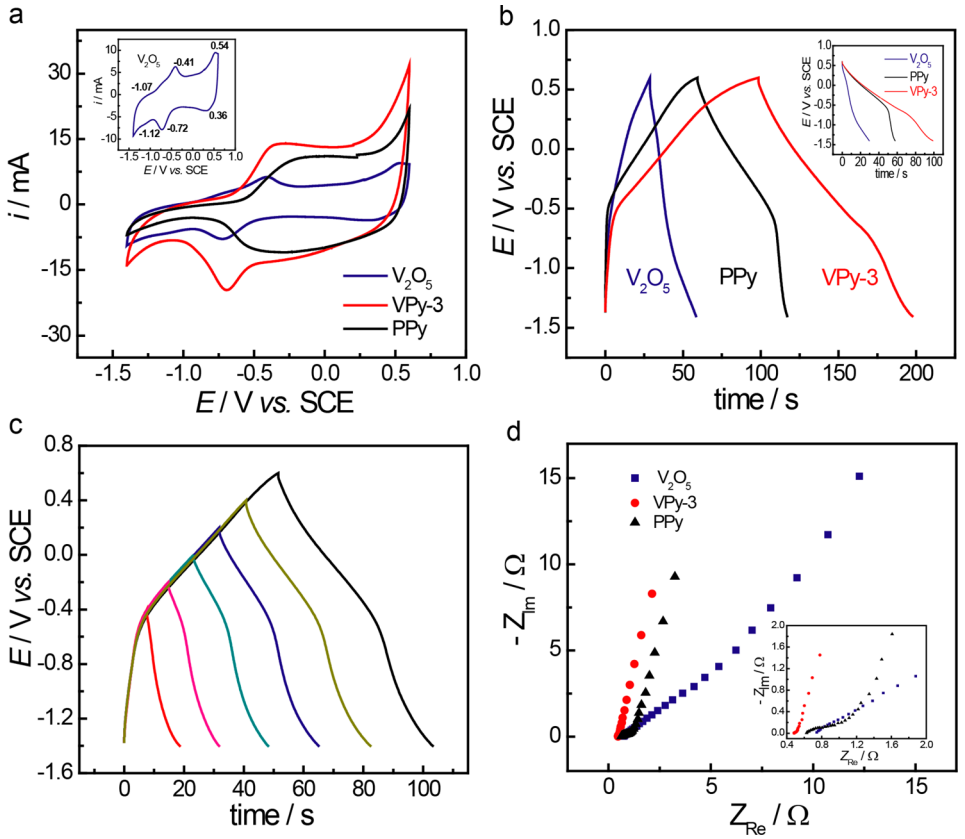

Figure 3. Electrochemical performance of VPy-3, V_2O_5, and PPy in 5 M LiCl solution. (a) CV profiles collected at a scan rate of 20 mV/s. (b) Galvanostatic charge−discharge profiles collected at a current density of 4.5 mA/cm^2. (c) Galvanostatic charge/discharge profiles of VPy-3 collected at different potentials at 9 mA/cm^2. (d) Nyquist plots of VPy-3, V_2O_5, and PPy; the high-frequency domain of the Nyquist plots is shown in the inset.

To study the electrochemical activities of VPy-3, cyclic voltammetry (CV) and chronopotentiometry (CP) experiment were conducted in 5 M LiCl aqueous electrolyte. The obtained CV and CP profiles are in Figure 3a and b, together with those of V_2O_5 and PPy. The inset in Figure 3a is the CV profile of V_2O_5 in enlarged scale, three redox pairs can be seen at −1.12/−1.07, −0.72/−0.41, and 0.36/0.54 V, respectively. It was reported that a V_2O_5 xerogel film displayed a redox pair at −0.76/−0.39 V vs Ag/AgCl which was ascribed by the authors to the Li^+ insertion/extraction into/out of V_2O_5 ($V_2O_5 + xLi^+ + xe^- \rightleftarrows Li_xV_2O_5$). This film also displayed a redox pair at ca. −1.13/−0.8 V, although much less noticeable.[31] Except redox pairs in negative potentials, a V_2O_5 sample made through a wet process also displayed a redox pair in positive potentials at ca.0.4/0.6 V.[32] The redox behaviors of our V_2O_5 sample (inset of Figure 3a) can be similarly ascribed to the formation of different crystalline phases of $Li_xV_2O_5$.[32] The electroactivities from −1.4 to 0.5 V endows the electrodeposited V_2O_5 wider charge storage potential window. Similar to the "ladder-doped" polypyrrole reported by Ingram and co-workers,[19] the PPy in this work displays a dual mode in its CV profile from −0.7 to 0.6 V (Figure 3a), which corresponding to the cation-involved and anion-involved electrochemistry processes, respectively. The CV profile of VPy-3 shows a combined shape of PPy and V_2O_5, proving the successful incorporation of V_2O_5 into PPy. Due to the combined electroactivities of PPy and V_2O_5, VPy-3 exhibits higher electroactivities and more importantly, a wide charge storage potential window of 2.0 V from −1.4 to 0.6 V vs SCE.

As can be seen in Figure 3b which presents the galvanostatic charge/discharge profiles obtained by CP at 4.5 mA cm^{-2} in 5 M LiCl aqueous electrolyte, PPy displays charge storage abilities in potentials from −0.7 to 0.6 V. After incorporation of V_2O_5 in the polymer, the obtained composite VPy-3 displays an extended charge storage potential window of 2.0 V (−1.4 to 0.6 V).

Figure 3c shows the CP profiles of VPy-3 collected at different potentials at a fixed current density of 9 mA/cm^2. The CP profiles approximately follow the same trace for charging, suggesting that the stable charge/discharge potential window of VPy-3 could be extended to 2.0 V from −1.4 to 0.6 V and hydrogen evolution is effectively inhibited. The effective hydrogen evolution inhibition was also detected on a free-standing polypyrrole film.[33] The specific capacitance can be calculated based on galvanostatic charge/discharge data according to eq 1.

$$C_s = I \times \Delta t/(\Delta U \times m) \quad (1)$$

In eq 1, C_s, I, Δt, ΔU, and m are specific capacitance (F/g), charge/discharge current (A) and time (s), discharge potential window (V), and mass loading of film (g), respectively. The C_s of VPy-3 is calculated to be 412 F g^{-1}, which is substantially higher than those of V_2O_5 (181 F/g) and PPy (257 F/g), consistent with CV analysis.

Electrochemical impedance characteristics of VPy-3, V_2O_5 and PPy are investigated at open circuit potential in 5 M LiCl. The Nyquist diagrams in the range of 40 kHz to 100 mHz are shown in Figure 3d. A slope of a nearly vertical line arises from

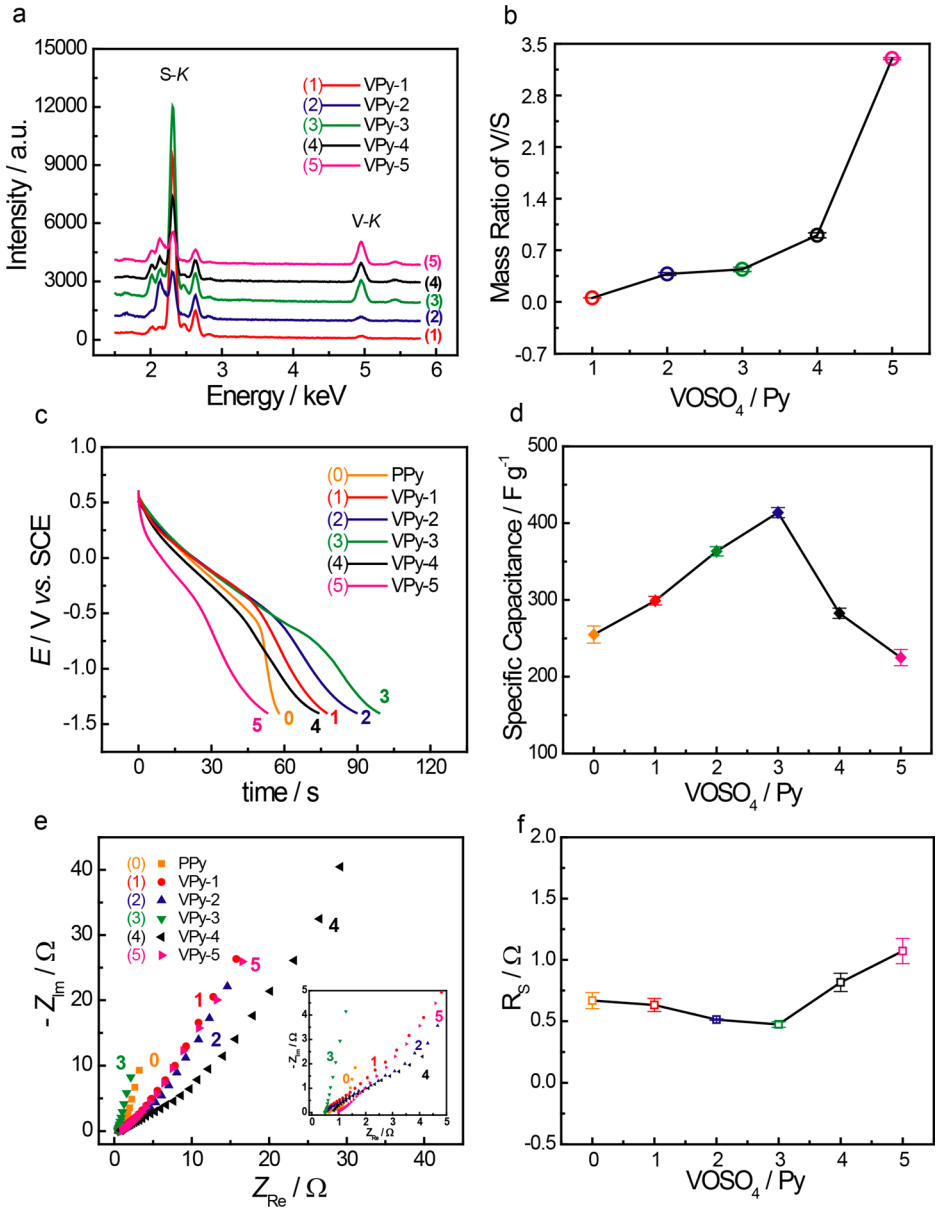

Figure 4. (a) EDX spectra of V_2O_5–PPy composites. (b) Mass ratio of V/S for V_2O_5–PPy composites electrodeposited in solutions containing $VOSO_4$ and Py in different concentration ratios, based on the data of three spot analyses for each film. (c) Galvanostatic discharge profiles at a current density of 4.5 mA/cm^2 from −1.4 to 0.6 V vs SCE in 5 M LiCl aqueous solution. (d) Plots of specific capacitance of composites made in solutions containing $VOSO_4$ and Py in different concentration ratios, based on the experiments on three films for each composite made under the same condition. (e) Nyquist plots of V_2O_5–PPy composites; the high-frequency domain of the Nyquist plots are shown in the inset. (f) Combined series resistance of composites made in solutions containing $VOSO_4$ and Py in different concentration ratios, based on the experiments on three films for each composite made under the same condition.

higher frequency for VPy-3 than for V_2O_5 and PPy, indicating the improved capacitive properties for the composite.[18,34] Inset of Figure 3d shows the high-frequency domain of the Nyquist plots. VPy-3 displays lower combined series resistance than PPy and V_2O_5, suggesting that its electrical conductivity has been improved.[35]

To further optimize the performance of V_2O_5–PPy composite, we investigated the influence of $VOSO_4$ to polypyrrole (Py) ratio in the electro-codeposition solution on properties of the obtained V_2O_5–PPy composites. Composites of VPy-1, VPy-2, VPy-3, VPy-4 and VPy-5 were synthesized from 0.1 M $VOSO_4$ solutions containing 0.1, 0.05, 0.03, 0.025, 0.02 M pyrrole, respectively. The energy-dispersive X-ray spectra (EDX) of the obtained V_2O_5–PPy composite films are in Figure 4a. In the EDX spectra, V signal came from V_2O_5, while S signal originated from SO_4^{2-} ions doped in the polymer. Assuming the doping level of PPy in all of the five composites is similar, the amount of SO_4^{2-} should be proportional to the amount of PPy. Then the mass ratio of V_2O_5 to PPy can be represented by the V/S mass ratio. As shown in Figure 4b, along with the decrease of the concentration of pyrrole in electrodeposition solution, the obtained composite displayed increased V/S ratio. This indicates that the ratio of V_2O_5 and PPy in the composite depends on the concentrations of $VOSO_4$ and pyrrole in the electrodeposition solution.

Galvanostatic charge–discharge experiments were conducted at a current density of 4.5 mA/cm^2 on the composites to

dx.doi.org/10.1021/am502630g | ACS Appl. Mater. Interfaces 2014, 6, 12656−12664

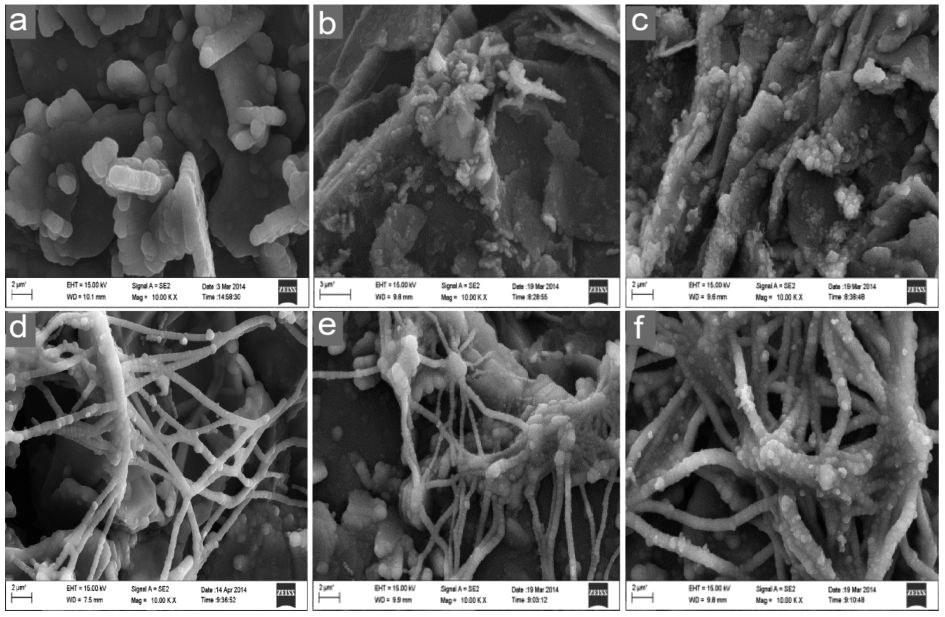

Figure 5. SEM images of (a) PPy, (b) VPy-1, (c) VPy-2, (d) VPy-3, (e) VPy-4 and (f) VPy-5.

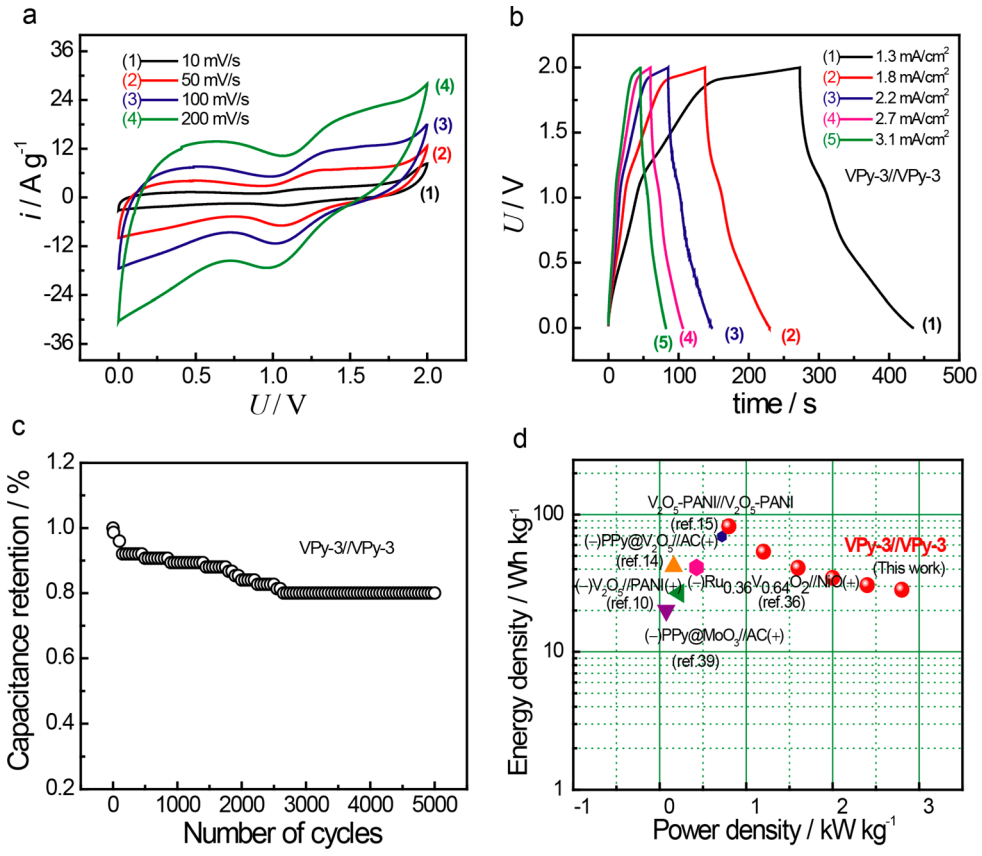

Figure 6. (a) CV profiles of VPy-3//VPy-3 type III composite supercapacitor measured between 0−2.0 V at various scan rates ranging from 10−200 mV/s. (b) galvanostatic charge−discharge profiles collected for VPy-3//VPy-3 type III composite supercapacitor at various current densities. (c) Cycling stability of VPy-3//VPy-3 collected by galvanostatic charge−discharge experiments at a current density of 9 mA/cm^2. (d) Ragone plots of VPy-3//VPy-3, the values reported for other supercapacitors are included for comparison.

evaluate their electrochemical performances. The obtained CP profiles are in Figure 4c, together with that of similarly prepared PPy. The VPy-3 sample displays the longest discharge time, indicating that it has the largest specific capacitance (Figure 4d). EIS measurements were conducted on the V_2O_5−PPy composites (Figure 4e). In the low-frequency domain of the Nyquist plots, VPy-3 displays a slope closer to 90° than others, exhibiting its best capacitive behavior.[18,34] Moreover, VPy-3 possesses the lowest combined series resistance, showing its improved electrical conductivity. The better performance of

dx.doi.org/10.1021/am502630g | ACS Appl. Mater. Interfaces 2014, 6, 12656−12664

VPy-3 over the other V_2O_5–PPy samples is supported by the EIS data.

To study the influence of $VOSO_4$/Py concentration ratio on composite electrodeposition, SEM was conducted to investigate morphologies of VPy-1, VPy-2, VPy-3, VPy-4, and VPy-5, together with that of PPy for comparison (Figure 5). The V_2O_5–PPy composites display smaller particles in their samples compared to PPy. This may be related to the effective restriction of PPy chain entanglement due to the adhered V_2O_5 particles, which prevent the polymer from further aggregation. Moreover, one-dimensional growth of PPy is directed when the $VOSO_4$ to Py ratio in the electro-codeposition solution is increased to 3 and upward (Figure 5d–f). Due to the increased specific surface area for the one-dimensional grown composites, which facilitates the effective contact of the reactive centers on the films with electrolyte, the one-dimensional composites should have higher specific capacitances. However, when more of the oxide is included in the composites to form VPy-4 and VPy-5, the specific capacitance decreases due to the lower contribution to specific capacitance by V_2O_5 (Figure 4d). In addition, the electric conductivity decrease with increasing oxide content in the composite, as shown in Figure 4f, would be another disadvantage.

To evaluate the performance of the VPy-3 composite in supercapacitors, a model type III composite supercapacitor VPy-3//VPy-3 was assembled using LiCl/PVA gel as electrolyte and two identical pieces of VPy-3 as anode and cathode, respectively. Cyclic voltammetry at various sweep rates and constant current charge/discharge measurements at different current densities were conducted on the model supercapacitor. The VPy-3//VPy-3 type III composite supercapacitor displays a good electrochemical capacitive behavior even at a high scan rate of 200 mV/s (Figure 6a), exhibiting fast charging/discharging property for power devices. The current–potential response is potential dependent due to the faradic process for charge storage. The typical galvanostatic charge–discharge profiles of the type III composite supercapacitor between 0.0 and 2.0 V at different current densities is shown in Figure 6b. The charge/discharge curves are not perfectly linear, showing the typical pseudocapacitive behavior with a slope variation of time dependence of the potential. Long-term stability of VPy-3//VPy-3 is investigated by constant current charge–discharge at 9 mA/cm^2 for 5000 cycles (Figure 6c). Eighty percent of the capacitance can be maintained after 5000 cycles for VPy-3//VPy-3, exhibiting its good cyclic charge–discharge stability. This is better than or comparable to the values reported by other groups for asymmetric supercapacitors using pseudocapacitive materials for both of the positive and negative electrodes, such as (−)V_2O_5//PANI(+) (73% after 2000 cycles),[10] (−)$Ru_{0.36}V_{0.64}O_2$//NiO(+) (83.5% after 1500 cycles),[36] (−)WO_3//RuO_2(+) (72% after 200 cycles),[37] and (−)WO_3–MoO_3//PANI(+) (75% after 5000 cycles).[38]

The specific capacitance of the model supercapacitor can be calculated according to eq 2 based on galvanostatic data in Figure 6b

$$C_m = I \times \Delta t/[U \times (m_{an} + m_{cat})] \quad (2)$$

where C_m, U, I, Δt, m_{an}, and m_{cat} are the specific capacitance (F/g) and operating voltage (V) of the model supercapacitor, charge/discharge current (A) and time (s), and mass loading on anode and cathode (g), respectively. The energy density and power density, which are important to evaluate supercapacitors, are calculated by eqs 3 and 4

$$E = 1/2C_m U^2 \quad (3)$$

$$P = 3600E/\Delta t \quad (4)$$

where E and P are the energy density (Wh/kg) and power density (W/kg), respectively, and C_m, U, and Δt are the specific capacitance (F/g), operating voltage (V), and discharge time (s), respectively. The results are summarized in Figure 6d. The VPy-3//VPy-3 achieved a high energy density of 82 Wh/kg at a power density of 0.8 kW/kg. The value is substantially higher than previously reported supercapacitors with acceptable cycling stability and using metal oxide-based pseudocapacitive materials as negative electrodes (Figure 6d), including our previously reported V_2O_5–PANI//V_2O_5–PANI device (69.2 Wh/kg at 0.72 kW/kg),[15] (−)V_2O_5//PANI(+) device (26.7 Wh/kg at 0.22 kW/kg),[10] (−)PPy@V_2O_5//AC(+) device (42 Wh/kg at 0.162 kW/kg),[14] (−)$Ru_{0.36}V_{0.64}O_2$//NiO(+) device (41.2 Wh/kg at 0.425 kW/kg),[36] and (−)PPy@MoO_3//AC(+) device (20 Wh/kg at 0.75 kW/kg).[39] The good performance of the supercapacitor can be attributed to the wide charge storage potential window and large pseudocapacitance of the VPy composite electrode.

CONCLUSIONS

A facile electro-codeposition method is used in this work to synthesize V_2O_5–PPy composite films on carbon cloth substrate through electrodeposition of V_2O_5 from vanadyl sulfate and electropolymerization of pyrrole simultaneously. One-dimensional growth of PPy was directed through this organic–inorganic electro-codeposition when the vanadyl sulfate to pyrrole ratio in the solution increases to 3:1. Thus, the obtained VPy-3 composite has a large surface area, which is beneficial for effective contact of reactive centers on the film to contact with electrolyte for charge storage. VPy-3 displayed a high specific capacitance of 412 F/g at a current density of 4.5 mA/cm^2. Significantly, the composite electrode displayed an exceptionally large charge storage potential window of 2.0 V from −1.4 to 0.6 V vs SCE, due to the combined electroactivities of the two components. Consequently, a type III composite supercapacitor VPy-3//VPy-3, assembled using VPy-3 as both of the electrodes, can work with a high operating voltage of 2 V and so display a high energy density of 82 Wh/kg at a power density of 800 W/kg. This model supercapacitor showed good cyclic charge–discharge stability; Eighty percent of the specific capacitance can be maintained after 5000 galvanostatic charge–discharge cycles. The energy density of VPy-3//VPy-3 is substantially higher than previously reported supercapacitors with acceptable cycling stability and using metal oxide-based pseudocapacitive materials as negative electrodes. In the assembled supercapacitor, although the same V_2O_5–PPy composite films were used as the electrode materials for both the anode and cathode, charges were stored through different electrochemistry processes in the anode and cathode. Thus, it provides a new type of asymmetric supercapacitor, very like the type III polymer supercapacitor in which charges are stored through *n*-doping and *p*-doping of the same polymer in anode and cathode, respectively. We think it is mainly due to the one-dimensional growth control of PPy through electro-codeposition with V_2O_5 and the significantly large charge storage potential window to make the V_2O_5–PPy composite a promising candidate for fabrication of high-performance supercapacitors.

AUTHOR INFORMATION

Corresponding Author

*E-mail: xxliu@mail.neu.edu.cn.

Notes

The authors declare no competing financial interest.

ACKNOWLEDGMENTS

We gratefully acknowledges supports of this work by National Natural Science Foundation of China (project number: 21273029) and Research Foundation for Doctoral Program of Higher Education of China (project number: 20120042110024).

REFERENCES

(1) Fan, Z.; Yan, J.; Wei, T.; Zhi, L.; Ning, G.; Li, T.; Wei, F. Asymmetric Supercapacitors Based on Graphene/MnO_2 and Activated Carbon Nanofiber Electrodes with High Power and Energy Density. *Adv. Funct. Mater.* **2011**, *21*, 2366−2375.

(2) Guan, Q.; Cheng, J.; Wang, B.; Ni, W.; Gu, G.; Li, X.; Huang, L.; Yang, G.; Nie, F. Needle-like Co_3O_4 Anchored on the Graphene with Enhanced Electrochemical Performance for Aqueous Supercapacitors. *ACS Appl. Mater. Interfaces* **2014**, *6*, 7626−7632.

(3) Peng, C.; Zhang, S.; Zhou, X.; Chen, G. Z. Unequalisation of Electrode Capacitances for Enhanced Energy Capacity in Asymmetrical Supercapacitors. *Energy Environ. Sci.* **2010**, *3*, 1499−1502.

(4) Wang, G.; Lu, X.; Ling, Y.; Zhai, T.; Wang, H.; Tong, Y.; Li, Y. LiCl/PVA Gel Electrolyte Stabilizes Vanadium Oxide Nanowire Electrodes for Pseudocapacitors. *ACS Nano* **2012**, *6*, 10296−10302.

(5) Lu, X.; Yu, M.; Zhai, T.; Wang, G.; Xie, S.; Liu, T.; Liang, C.; Tong, Y.; Li, Y. High Energy Density Asymmetric Quasi-Solid-State Supercapacitor Based on Porous Vanadium Nitride Nanowire Anode. *Nano Lett.* **2013**, *13*, 2628−2633.

(6) Wang, G.; Zhang, L.; Zhang, J. A Review of Electrode Materials for Electrochemical Supercapacitors. *Chem. Soc. Rev.* **2012**, *41*, 797−828.

(7) Yu, G.; Hu, L.; Vosgueritchian, M.; Wang, H.; Xie, X.; McDonough, J. R.; Cui, X.; Cui, Y.; Bao, Z. Solution-Processed Graphene/MnO_2 Nanostructured Textiles for High-Performance Electrochemical Capacitors. *Nano Lett.* **2011**, *11*, 2905−2911.

(8) Xiao, J.; Yang, S. Sequential Crystallization of Sea Urchin-like Bimetallic (Ni, Co) Carbonate Hydroxide and Its Morphology Conserved Conversion to Porous $NiCo_2O_4$ Spinel for Pseudocapacitors. *RSC Adv.* **2011**, *1*, 588−595.

(9) Li, J.-M.; Chang, K.-H.; Hu, C.-C. A Novel Vanadium Oxide Deposit for the Cathode of Asymmetric Lithium-ion Supercapacitors. *Electrochem. Commun.* **2010**, *12*, 1800−1803.

(10) Mak, W. F.; Wee, G.; Aravindan, V.; Gupta, N.; Mhaisalkar, S. G.; Madhavi, S. High-Energy Density Asymmetric Supercapacitor Based on Electrospun Vanadium Pentoxide and Polyaniline Nanofibers in Aqueous Electrolyte. *J. Electrochem. Soc.* **2012**, *159*, A1481−A1488.

(11) Chen, P.-C.; Shen, G.; Shi, Y.; Chen, H.; Zhou, C. Preparation and Characterization of Flexible Asymmetric Supercapacitors Based on Transition-Metal-Oxide Nanowire/Single-Walled Carbon Nanotube Hybrid Thin-film Electrodes. *ACS Nano* **2010**, *4*, 4403−4411.

(12) Wu, C.; Feng, F.; Xie, Y. Design of Vanadium Oxide Structures with Controllable Electrical Properties for Energy Applications. *Chem. Soc. Rev.* **2013**, *42*, 5157−5183.

(13) Zhu, J.; Cao, L.; Wu, Y.; Gong, Y.; Liu, Z.; Hoster, H. E.; Zhang, Y.; Zhang, S.; Yang, S.; Yan, Q.; Ajayan, P. M.; Vajtai, R. Building 3D Structures of Vanadium Pentoxide Nanosheets and Application as Electrodes in Supercapacitors. *Nano Lett.* **2013**, *13*, 5408−5413.

(14) Qu, Q.; Zhu, Y.; Gao, X.; Wu, Y. Core-Shell Structure of Polypyrrole Grown on V_2O_5 Nanoribbon as High Performance Anode Material for Supercapacitors. *Adv. Energy Mater.* **2012**, *2*, 950−955.

(15) Bai, M.-H.; Liu, T.-Y.; Luan, F.; Li, Y.; Liu, X.-X. Electrodeposition of Vanadium Oxide−Polyaniline Composite Nanowire Electrodes for High Energy Density Supercapacitors. *J. Mater. Chem. A* **2014**, *2*, 10882−10888.

(16) Ferraris, J. P.; Gottesfeld, S.; Rudge, A. J., Electrochemical Supercapacitors. U.S. Patent 5,527,640, Jun. 18, 1996.

(17) Yuan, L.; Yao, B.; Hu, B.; Huo, K.; Chen, W.; Zhou, J. Polypyrrole-Coated Paper for Flexible Solid-State Energy Storage. *Energy Environ. Sci.* **2013**, *6*, 470−476.

(18) Davies, A.; Audette, P.; Farrow, B.; Hassan, F.; Chen, Z.; Choi, J.-Y.; Yu, A. Graphene-Based Flexible Supercapacitors: Pulse-Electropolymerization of Polypyrrole on Free-Standing Graphene Films. *J. Phys. Chem. C* **2011**, *115*, 17612−17620.

(19) Ingram, M. D.; Staesche, H.; Ryder, K. 'Ladder-Doped' Polypyrrole: A Possible Electrode Material for Inclusion in Electrochemical Supercapacitors? *J. Power Sources* **2004**, *129*, 107−112.

(20) Zhang, X.; Manohar, S. K. Bulk Synthesis of Polypyrrole Nanofibers by a Seeding Approach. *J. Am. Chem. Soc.* **2004**, *126*, 12714−12715.

(21) Nguyen, T. D.; Pham, M.; Piro, B.; Aubard, J.; Takenouti, H.; Keddam, M. Conducting Polymers and Corrosion PPy—PPy-PDAN Composite Films Electrosynthesis and Characterization. *J. Electrochem. Soc.* **2004**, *151*, B325−B330.

(22) Zhang, D.; Zhang, X.; Chen, Y.; Yu, P.; Wang, C.; Ma, Y. Enhanced Capacitance and Rate Capability of Graphene/Polypyrrole Composite as Electrode Material for Supercapacitors. *J. Power Sources* **2011**, *196*, 5990−5996.

(23) Guanggui, C.; Jianning, D.; Zhongqiang, Z.; Zhiyong, L.; Huasheng, P. Study on the Preparation and Multiproperties of the Polypyrrole Films Doped with Different Ions. *Surf. Interface Anal.* **2012**, *44*, 844−850.

(24) Perera, S. D.; Patel, B.; Nijem, N.; Roodenko, K.; Seitz, O.; Ferraris, J. P.; Chabal, Y. J.; Balkus, K. J. Vanadium Oxide Nanowire - Carbon Nanotube Binder - Free Flexible Electrodes for Supercapacitors. *Adv. Energy Mater.* **2011**, *1*, 936−945.

(25) Huang, J.; Kaner, R. B. A General Chemical Route to Polyaniline Nanofibers. *J. Am. Chem. Soc.* **2004**, *126*, 851−855.

(26) Huang, J.; Kaner, R. B. The Intrinsic Nanofibrillar Morphology of Polyaniline. *Chem. Commun.* **2006**, 367−376.

(27) Lu, X.; Mao, H.; Chao, D.; Zhang, W.; Wei, Y. Fabrication of Polyaniline Nanostructures under Ultrasonic Irradiation: From Nanotubes to Nanofibers. *Macromol. Chem. Phys.* **2006**, *207*, 2142−2152.

(28) Chiou, N. R.; Epstein, A. J. Polyaniline Nanofibers Prepared by Dilute Polymerization. *Adv. Mater.* **2005**, *17*, 1679−1683.

(29) Martin, C. R. Nanomaterials: A Membrane-Based Synthetic Approach. *Science* **1994**, *266*, 1961−1965.

(30) Yang, Y.; Liu, J.; Wan, M. Self-Assembled Conducting Polypyrrole Micro/Nanotubes. *Nanotechnology* **2002**, *13*, 771−773.

(31) Liu, D.; Liu, Y.; Candelaria, S. L.; Cao, G.; Liu, J.; Jeong, Y.-H. Atomic Layer Deposition of Al_2O_3 on V_2O_5 Xerogel Film for Enhanced Lithium-ion Intercalation Stability. *J. Vac. Sci. Technol. A* **2012**, *30*, 01A123−1-6.

(32) Nagase, K.; Shimizu, Y.; Miura, N.; Yamazoe, N. Electrochromic Properties of Vanadium Pentoxide Thin Films Prepared by New Wet Process. *Appl. Phys. Lett.* **1992**, *60*, 802−804.

(33) Otero, T. F.; Martinez, J. G.; Fuchiwaki, M.; Valero, L. Structural Electrochemistry from Freestanding Polypyrrole Films: Full Hydrogen Inhibition from Aqueous Solutions. *Adv. Funct. Mater.* **2014**, *24*, 1265−1274.

(34) Chang, H.-H.; Chang, C.-K.; Tsai, Y.-C.; Liao, C.-S. Electrochemically Synthesized Graphene/Polypyrrole Composites and their Use in Supercapacitor. *Carbon* **2012**, *50*, 2331−2336.

(35) Kim, M.; Hwang, Y.; Min, K.; Kim, J. Concentration Dependence of Graphene Oxide−Nanoneedle Manganese Oxide Composites Reduced by Hydrazine Hydrate for an Electrochemical Supercapacitor. *Phys. Chem. Chem. Phys.* **2013**, *15*, 15602−15611.

(36) Yuan, C.-Z.; Gao, B.; Zhang, X.-G. Electrochemical Capacitance of NiO/$Ru_{0.35}V_{0.65}O_2$ Asymmetric Electrochemical Capacitor. *J. Power Sources* **2007**, *173*, 606−612.

(37) Chang, K.-H.; Hu, C.-C.; Huang, C.-M.; Liu, Y.-L.; Chang, C.-I. Microwave-Assisted Hydrothermal Synthesis of Crystalline WO_3−WO_3·0.5H_2O Mixtures for Pseudocapacitors of the Asymmetric Type. *J. Power Sources* **2011**, *196*, 2387−2392.
(38) Xiao, X.; Ding, T.; Yuan, L.; Shen, Y.; Zhong, Q.; Zhang, X.; Cao, Y.; Hu, B.; Zhai, T.; Gong, L. WO_{3-x}/MoO_{3-x} Core/Shell Nanowires on Carbon Fabric as an Anode for All-Solid-State Asymmetric Supercapacitors. *Adv.Energy Mater.* **2012**, *2*, 1328−1332.
(39) Liu, Y.; Zhang, B.; Yang, Y.; Chang, Z.; Wen, Z.; Wu, Y. Polypyrrole-Coated α-MoO_3 Nanobelts with Good Electrochemical Performance as Anode Materials for Aqueous Supercapacitors. *J. Mater. Chem. A* **2013**, *1*, 13582−13587.